CHEMISTRY OF MATERIALS

Article

pubs.acs.org/cm

Tuning Two-Photon Absorption Cross Section in Metal Organic Frameworks

Hong Sheng Quah,[†] Venkatram Nalla,[‡] Kezhi Zheng,[†] Chloe Aloycia Lee,[†] Xiaogang Liu,[†] and Jagadese J. Vittal*[,†]

[†]Department of Chemistry, National University of Singapore, 3 Science Drive 3, Singapore 117543

[‡]Centre for Disruptive Photonic Technologies (CDPT), School of Physical and Mathematical Sciences, Nanyang Technological University, Singapore 637371

Supporting Information

ABSTRACT: The development of alternative nonlinear optical metamaterials has attracted much attention recently due to technological demands. Upconversion emission via a simultaneous two-photon absorption process is a nonlinear process that is widely studied in synthetically challenging organic compounds. Hereby, we report 9 metal organic frameworks constructed with various combinations of the following ligands: *trans*,*trans*-9,10-bis(4-pyridylethenyl) anthracene, *trans*,*trans*-9,10-bis(4-pyridylethynyl) anthracene, 1,4-bis[2-(4′-pyridyl)ethenyl]benzene, 4,4′-stilbene dicarboxylate, 4,4′-biphenyl dicarboxylate, 4,4′-benzene dicarboxylate, and benzene-1,3,5-tricarboxylate. Altering the auxiliary carboxylate ligands not only changes the structure but also varies the two-photon excited fluorescence. The two-photon excited emission is enhanced when longer spacer ligands are used and when they are packed in more expanded structures in **hms** topology. Unusually, the emission becomes stronger when a pair of pyridyl type ligands are perfectly aligned in parallel which could be due to reduction in nonradiative decay caused by molecular rotation. The comparison of two-photon absorption cross sections with their action cross section counterpart revealed a dissimilar trend. High level of absorption in MOFs does not necessitate the formation of a highly excited emissive state. To the best of our knowledge, this is the first example of a systematic structural−property relationship study on the two-photon excited fluorescence in metal organic frameworks.

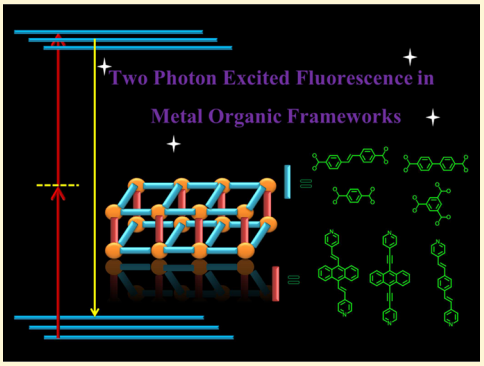

INTRODUCTION

Two-photon responsive materials are attractive as they are the key to high density storage materials, high contrast bioimaging, and optical lasing and limiting.[1−4] In contrast to linear excitation, fluorescence yielded from two-photon excitation offers better contrast and depth of penetration within the material.[5] This third-order nonlinear optical property is commonly observed in organic dyes which consist of highly conjugated structures that facilitate either a symmetrical structure of donor−π−acceptor−π−donor (D−π−A−π−D) or acceptor−π−donor−π−acceptor (A−π−D−π−A) arrangement.[6] An asymmetrical variant of the structure (A−π−D) can similarly provide the necessary intramolecular charge transfer which affects the compound's second hyperpolarizability, γ.[7,8] Typically, the two-photon absorption (TPA) cross section σ is proportional to the imaginary part of the second order hyperpolarizability.[9] The hyperpolarizability can further be boosted if the compound consists of a biradical ground state.[10−13] Overall, these governing principles provided the basis to design discrete molecules with high two-photon absorption cross section which is a measure of the material's nonlinear susceptibility. Nonetheless, organic materials are more susceptible to oxidation, photodegradation, and photobleaching compared to inorganic compounds. On the other hand, inorganic materials which offer stability such as silica and semiconductors do not offer broad band two-photon absorption emission as do their organic counterparts. Bearing in mind the respective materials' limitations, metal organic frameworks (MOFs) have emerged as the most suitable candidate for the required enhanced stability and tunability offered by both the metal ions and organic ligand, respectively.

Metal organic frameworks (MOFs) are a class of crystalline compounds widely investigated for a myriad of applications as they often combine the advantages offered by the metal ions and organic spacers.[14] Properties such as gas storage[15] and separation,[16] luminescence,[17] catalysis,[18] magnetism,[19] and conductivity[20] have been well-documented in the literature. Recently, Qian et al. demonstrated the first two-photon responsive MOFs by spacing a zwitterionic ligand between zinc ions.[21] Subsequently, we recorded the enhancement of multiple-photon-excited fluorescence via a host−guest energy transfer strategy using the ligand *trans*,*trans*-9,10-bis(4-pyridylethenyl) anthracene (An2Py).[22] Hereby, we extend the study with the synthesis and characterization of a series of novel

Received: June 11, 2017
Revised: August 15, 2017
Published: August 28, 2017

DOI: 10.1021/acs.chemmater.7b02417
Chem. Mater. 2017, 29, 7424−7430

Scheme 1. Reaction Scheme of Compounds 1−9 Synthesized and Studied in This Paper

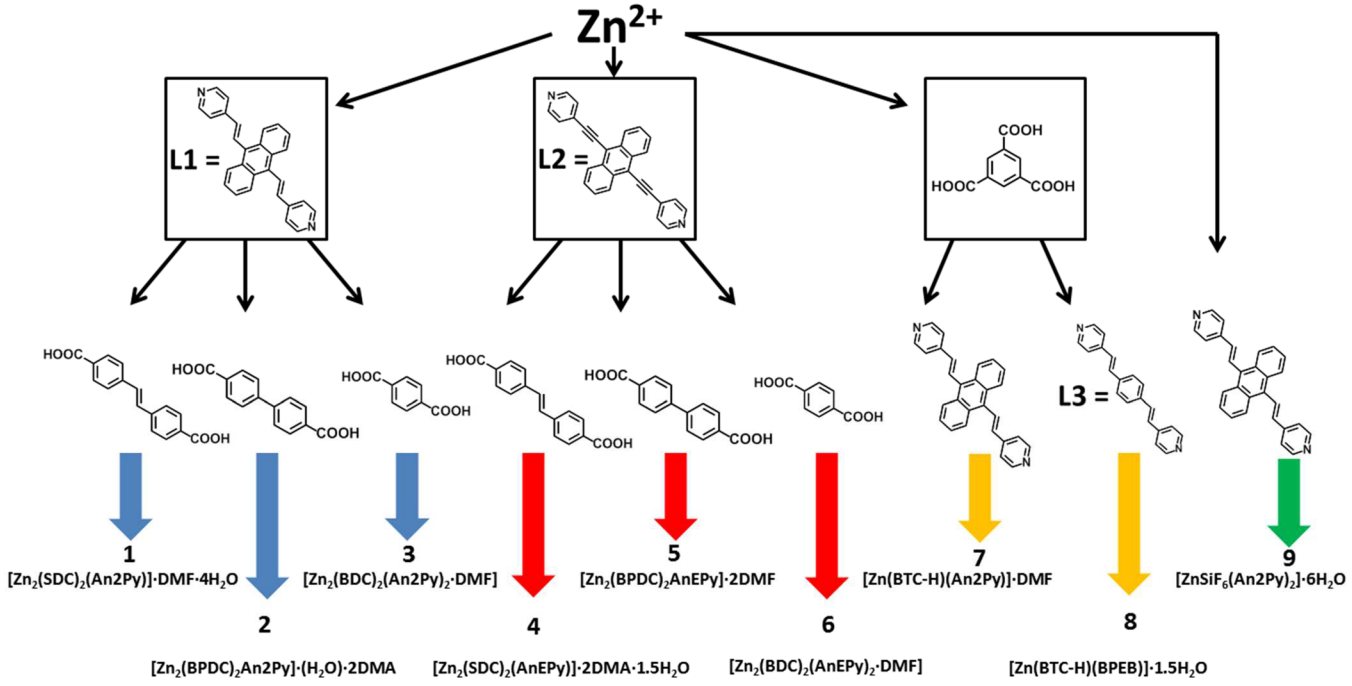

zinc-based MOFs using *trans,trans*-9,10-bis(4-pyridylethenyl) anthracene (L1 = An2Py), *trans,trans*-9,10-bis(4-pyridylethynyl) anthracene (L2 = AnEPy), 1,4-bis[2-(4′-pyridyl)ethenyl]-benzene (L3 = BPEB), 4,4′-stilbene dicarboxylic acid (H_2SDC), 4,4′-biphenyl dicarboxylic acid (H_2BPDC), 4,4′-benzene dicarboxylic acid (H_2BDC), and benzene-1,3,5-tricarboxylic acid (H_3BTC). The details of their variation and combination in assembling MOFs are reflected in Scheme 1. The two-photon excited emissions of these newly synthesized MOFs are compared to those of the previously reported compounds **1**,[22] **5**,[23] and **6**[24] reproduced in this paper to understand their structural−property relationship. Unlike organic chromophores, the effect of structural variation of MOFs on two-photon excited emission is explored.

EXPERIMENTAL SECTION

Synthesis. Compounds **1**, **5**, and **6** are reproduced by a previously reported procedure.[22−24]

[Zn_2(SDC)$_2$(An2Py)]·DMF·4H_2O, 1. Compound **1** was reproduced by our previously reported procedure. Bright yellow plate-like crystals were obtained and washed with DMF.

[Zn_2(BPDC)$_2$(An2Py)]·2DMA·1H_2O, 2. Compound **2** was prepared solvothermally by reacting $Zn(ClO_4)_2·6H_2O$ (4.65 mg, 0.0125 mmol), H_2BPDC (6.1 mg, 0.025 mmol), and An2Py (4.8 mg, 0.0125 mmol) in 3 mL of dimethylacetamide (DMA) and 1 mL of H_2O at 120 °C for 2 days. Yellow platy crystals of **2** were obtained, which were filtered and dried. Yield (47%). Elemental analysis for desolvated **2** (%). Calcd: C, 67.28; H, 4.03; N, 2.8. Found: C, 66.12; H, 3.71; N, 3.55.

[Zn_2(BDC)$_2$(An2Py)$_2$·DMF], 3. Compound **3** was prepared solvothermally by reacting $Zn(ClO_4)_2·6H_2O$ (4.65 mg, 0.0125 mmol), H_2BDC (2.1 mg, 0.025 mmol), and An2Py (4.80 mg, 0.0125 mmol) in 3 mL of dimethylformamide (DMF) and 1 mL of H_2O at 120 °C for 2 days. Orange rectangular single crystals of **3** were obtained, which were filtered and dried. Yield (65%). Elemental analysis for desolvated **3** (%). Calcd: C, 70.19; H, 4.25; N, 4.55. Found: C, 68.81; H, 3.95; N, 5.43.

[Zn_2(SDC)$_2$(AnEPy)]·2DMA·1.5H_2O, 4. Compound **4** was prepared solvothermally by reacting $Zn(ClO_4)_2$ (9.3 mg, 0.025 mmol), 4.8 mg (0.0125 mmol) of AnEPy, and 6.7 mg (0.025 mmol) of H_2SDC in a 25 mL scintillating vial. A total of 2 mL of DMA and 1 mL of water was added to the solids with a drop of HNO_3. The bright red solution that formed in the vial was capped and heated in the oven for 2 days at 120 °C followed by slow cooling. Brown plate-like crystals were obtained and washed with DMF. Yield (40%). Elemental analysis for desolvated **4** (%). Calcd: C, 68.78; H, 3.85; N, 2.67. Found: C, 68.49; H, 3.81; N, 3.71.

[Zn_2(BPDC)$_2$AnEPy]·(DMF)$_2$, 5. Compound **5** was reproduced from the reported procedure. Brown platy crystals of **5** were obtained, which were filtered and dried. Yield (57%). Elemental analysis for **5** (%). Calcd: C, 65.45; H, 4.07; N, 4.92. Found: C, 64.61; H, 4.37; N, 5.22.

[Zn_2(BDC)$_2$(AnEPy)$_2$·DMF], 6. Compound **6** was reproduced from the reported procedure. Brown rectangular single crystals of **6** were obtained, which were filtered and dried. Yield (52%). Elemental analysis for **6** (%). Calcd: C, 69.67; H, 3.66; N, 5.42. Found: C, 68.37; H, 3.77; N, 5.51.

[Zn(BTC-H)(An2Py)]·DMF, 7. Compound **7** was prepared solvothermally by reacting $Zn(ClO_4)_2·6H_2O$ (4.65 mg, 0.0125 mmol), H_3BTC (5.25 mg, 0.025 mmol), and An2Py (9.6 mg, 0.025 mmol) in 3 mL of dimethylformamide (DMF) and 1 mL of H_2O at 120 °C for 2 days. Yellow hexagonal crystals of **7** were obtained, filtered, and further dried. Yield (61%). Elemental analysis (%). Calcd: C, 65.53; H, 4.54; N, 5.73. Found: C, 64.64; H, 4.49; N, 5.76.

[Zn(BTC-H)(BPEB)]·1.5H_2O, 8. Compound **8** was prepared solvothermally by reacting $Zn(ClO_4)_2·6H_2O$ (4.65 mg, 0.0125 mmol), H_3BTC (2.6 mg, 0.012 mmol), and BPEB (3.5 mg, 0.012 mmol) in 3 mL of dimethylformamide (DMF) and 1 mL of H_2O at 120 °C for 2 days. Yellow crystals of **8** were obtained, which were filtered and dried. Yield (63%). Elemental analysis for desolvated **8** (%). Calcd: C, 62.21; H, 3.96; N, 5.00. Found: C, 62.46; H, 3.77; N, 5.41.

[$ZnSiF_6$(An2Py)$_2$]·6H_2O, 9. A total of 0.5 mL of $ZnSiF_6$ (0.1 mmol in 4 mL of dry MeOH) was layered over 2 mL of An2Py (4.8 mg in 2 mL of THF) with 2 mL of MeOH buffer. After 4 days, orange crystals were obtained and filtered. Yield (53%). Elemental analysis for desolvated **9** (%). Calcd: C, 68.89; H, 4.13; N, 5.74. Found: C, 66.35; H, 4.2; N, 5.96.

DOI: 10.1021/acs.chemmater.7b02417
Chem. Mater. 2017, 29, 7424−7430

RESULTS

Single Crystals Analysis. A section of the crystal structure packing of compounds **1**−**9** is shown in Figure 1 for easy comparison. Detailed structural analysis is shown in Supporting Information Figures S1−6. Compounds **1**−**3** are assembled principally using An2Py. Compounds **1**, **5**, and **6** were previously reported but are reproduced here to compare the relative two-photon emission strengths of these compounds. **1** adopts a 3D 4-fold interpenetrated **pcu** net that comprised of a paddle-wheel building unit and has a 36.2% void.[22] Similarly, compound **2** crystallized in a monoclinic $C2/c$ space group with $Z = 4$ and is assembled into a 3D 4-fold interpenetrated **pcu** net that is comprised of a paddle-wheel building unit. The asymmetric unit contains half of the formula unit. The building block or the repeating unit is made up of paddlewheels that are connected by BPDC to form a layer. The axial positions are occupied by An2Py pillars with a center-to-center distance along the An2Py ligand of 22.969 Å. The $[Zn_2(BPDC)_2]$ layer consists of rhomboidal shape with a length of 15.148 Å and angle of 86.4°. It has a theoretical void space of 25.9% as calculated by PLATON. Compound **3** crystallized in a triclinic space group $P\bar{1}$ with $Z = 2$, which has a double pillared-layer structure with a 3D 2-fold interpenetrated **pcu** topology. The An2Py ligands are spanned along the c-axis, and, hence, the repeating distance is 20.352 Å. The (4,4) layer formed by the $[Zn_2(BDC)_2]$ parallelogram with the Zn-BDC-Zn projected along a- and b-axes of the unit cell. The two An2Py ligands in the double pillars are in parallel, although the ligand is not coplanar. The center-to-center distances of the olefin pairs are 3.882 and 3.889 Å. However, no photocyclization has been observed in these ligands so far. Its theoretical void is determined to be 13.4%.

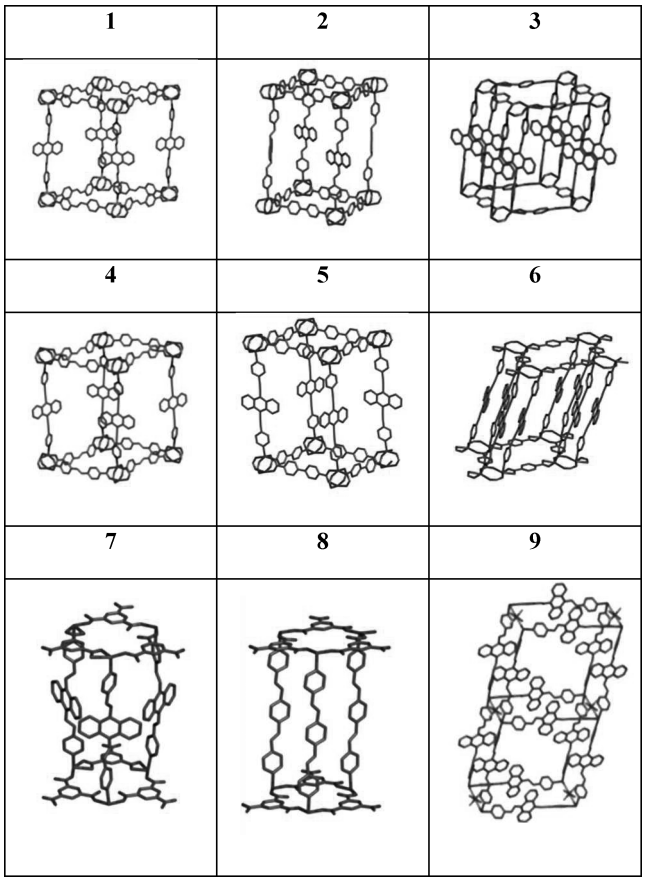

Figure 1. X-ray single crystal structures of compounds **2**−**4** and **7**−**9**. Reported structures are drawn for **1** and **5**−**6**.

Compounds **4**−**6** are assembled principally using AnEPy. Instead of a double bond spacing the pyridyl group and the anthracene, this ligand is spaced by a triple bond. Compound **4** is the analogue of **1**, and it crystallized in a similar space group with $Z = 4$ and is a 3D 4-fold interpenetrated **pcu** net. The asymmetric unit has half of the paddlewheel repeating unit. The crystals of **4** are isomorphous to **1** and **2**, and, hence, the structural description is very similar to those of these two compounds. The center-to-center distance along the An2Py ligand is 23.323 Å. The $[Zn_2(SDC)_2]$ layer consists of rhomboidal shape with a length of 17.248 Å and angle of 77.4°. The SDC ligands are highly puckered. Its theoretical void is determined to be 39.1%. As compounds **5** and **6** are previously reported, they were found to be analogues of **2** and **3**; they have the same connectivity and interpenetration. Their voids were calculated to be 23% and 13.1%, respectively.

Extending further, compounds **7** and **8** are assembled principally with benzene-1,3,5-tricarboxylic acid (H_3BTC). Compound **7** is made with An2Py while **8** is constructed with the benzene analogue of An2Py, BPEB. While **7** crystallized in a trigonal space group $P\bar{3}1c$ with $Z = 12$, **8** belongs to a monoclinic space group Pc with $Z = 2$. The asymmetric unit of **7** contains one formula unit. The chemical composition indicates that one proton in H_3BTC was not removed in **7**. The geometry and distance of 2.485 Å between noncoordinated O4 and O6 atoms indicated that these two atoms are hydrogen bonded. The C28−O4 distance of 1.273(10) Å is longer than C28−O3 of 1.247(9) Å. Further, O3 is bonded to Zn1 (2.031(6) Å), and hence it is concluded that C28−O3 is a carbonyl, C═O bond, and the O6 atom is protonated. The Zn1 atom has highly distorted octahedral geometry with the two pyridyl groups bonded at the axial positions. The An2Py ligand is traversed along the c-axis, and the Zn−An2Py−Zn distance of 20.190 Å is half of the length of the c-axis (40.371(10) Å. Further, the Zn(BTC-H) interactions constitute a layer in the ab-plane. Due to the 1,3,5 positions of the CO_2 fragments on the benzene ring, the Zn(II) are surrounded the BTC-H ligand forming a equilateral triangle with a separation of 9.380 Å. They are further linked forming another triangle with side lengths of 9.380, 9.846, and 10.048 Å. On the other hand, one of the carboxylic acids for **8** is not deprotonated in BTC as observed in **7**. The two repeating units of the interpenetrated structures are crystallographically independent in the asymmetric unit. Otherwise, the structural description is very similar to that of **7**. The geometry and distance between noncoordinated O4 and O5 atoms in the first building unit and O8 and O9 atoms in the second building unit indicated that they are hydrogen bonded. It appears that the acidic proton might be in the middle of these O atoms as the C−O distance did not clearly favor the clear association of H on one O atom in these two repeating units. The Zn1 atom has highly distorted octahedral geometry with the two pyridyl groups bonded at the axial positions. The BPEB ligand is navigated along the a-axis, and the Zn−An2Py−Zn distance is the same as the length of the a-axis (20.193(9)) Å. Further, the Zn(BTC-H) interactions constitute a layer in the bc-plane. Due to the 1,3,5 positions of the CO_2 fragments on the benzene ring, the Zn(II) are surrounded the BTC-H ligand forming equilateral triangles, and these are further linked forming

DOI: 10.1021/acs.chemmater.7b02417
Chem. Mater. 2017, 29, 7424−7430

another set of triangles. Despite the different pillar ligand, the MOFs **7** and **8** crystallized in a similar doubly interpenetrated **hms** net with voids 20.1% and 33.2%, respectively. The Zn(II) ions in both compounds are connected by three BTC ligands forming an extended two-dimensional net. The net is further pillared by An2Py or BPEB forming the **hms** net.

Instead of using the auxiliary organic spacer, an inorganic anionic hexafluorosilicate yielded **9** together with Zn(II) and An2Py generating crystals that belong to the tetragonal space group $P4/ncc$ with $Z = 16$. The asymmetric unit contains 1/4 of the repeating unit. Each Zn(II) bonded to four N atoms of the An2Py ligands forming a plane and the axial positions are occupied by the F atoms of the SiF_6^{2-} ions. The Zn−An2Py−Zn distance is equal to *a*- and *b*-axes, and hence $[Zn(An2Py)_2]$ occupies the *ab*-plane. The Zn−SiF_6−Zn distance is half the length of the *c*-axis. Overall, it generates a two-dimensional square grid while the hexafluorosilicate anion pillars form the 3D **pcu** doubly interpenetrated net consisting of 37.1% void. This is similar to many compounds reported by Zaworotko and co-workers.[25]

Overall in **1**−**3**, by shortening the length of the carboxylate ligand from SDC to BPDC, the void space is decreased though there is no change in the overall topology, packing, and interpenetration. However, replacing BPDC with BDC led to both decreased interpenetration as well as void reduction. Since **4**−**6** are similar to **1**−**3**, the trend followed as expected. When the carboxylate ligand is varied from bidentate to a tridentate BTC, the topology is changed from **pcu** to **hms**. When hexafluorosilicate anion was used instead of BDC, the building unit changed from paddlewheel to a single ion six-coordinating zinc(II) center.

Single Photon Analysis. The single photon emission is obtained for all the compounds and is accompanied in Figure S27. The solid state emission spectra of An2Py, AnEPy, and BPEB exhibited emission maxima at 516, 540, and 558 nm. Compounds **1**−**9** correspondingly show emission maxima at 553, 531, 556, 560, 560, 581, 557, 520, and 624 nm.

Two-Photon Analysis. The compounds are then placed on a glass slide and excited with a pulsed laser at 800 nm on a confocal microscope setup. Since most compounds have absorption maxima at 400−500 nm (see Figures S25 and S26), the 800 nm excitation is a two-photon excited process. The confocal microscope captured the dark areas which are the nonactive two-photon region as shown in Figure 2. The emission spectra of the compounds are collected via the spectrometer connected to the microscope. A relative estimate of the two-photon action cross section strengths of the compounds is obtained by comparison of their emission spectra. Perylene is a known standard two-photon dye with a reported absorption cross section of 3.0 GM (3×10^{-50} $cm^4 \cdot s \cdot photon^{-1}$) at 800 nm, and its solid state (powder) quantum yield at is ∼0.18.[26,27] The relative two-photon action cross sections of the samples at 800 nm can be obtained from the previously employed proportion method by using the perylene standard.[22]

The equation used to generate the computation and their action cross sections are shown in Figure 3. The quantum yields were further obtained for the compounds to compute their relative absorption cross sections (Figure S35). The quantum yields and absorption cross section of the compounds are shown in Figure 4. Notably, the two-photon absorption action cross sections of **1**−**3** (1.95−3.09 GM) are notably higher than those of **4**−**6** (0.54−0.75 GM), while those of **7**−**9**

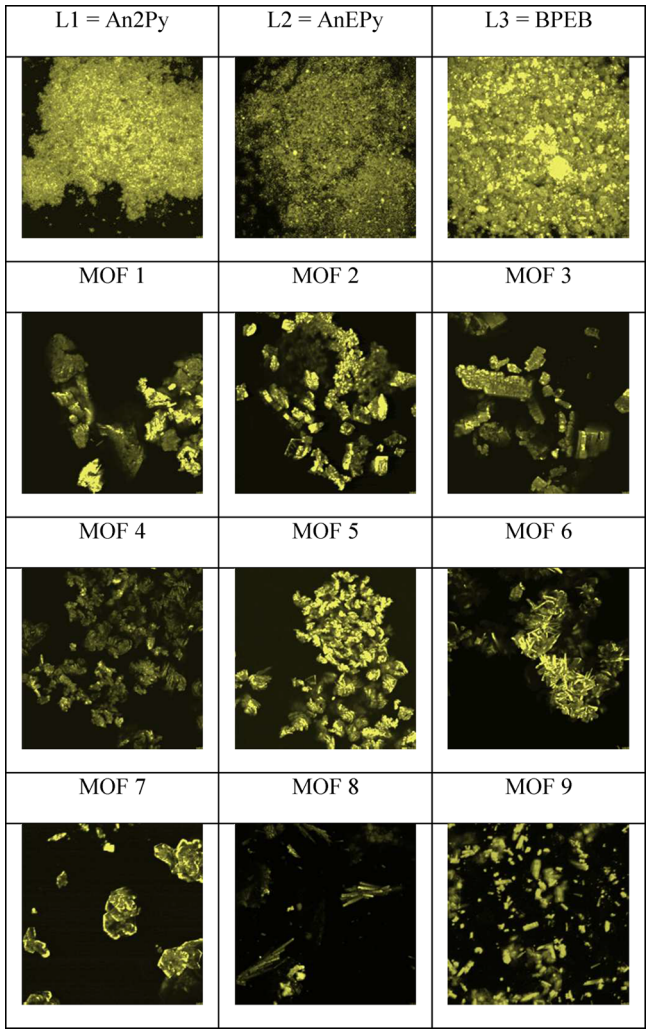

Figure 2. Confocal microscopic images of the ground ligands and compounds **1**−**9** under 800 nm pulsed laser excitation. The colors shown are arbitrarily represented as the intensities are measured by a photomultiplier tube counter.

generate values between 1.21 and 2.23 GM. The ligands L1−L3 fare lesser (0.14−0.21 GM) than the MOFs and standard perylene dye in the solid state.

On the other hand, the absorption cross section showed a different trend. L1−L3 showed values between 2.88 and 10.45 while the MOFs exhibited a wide range from 2.6 to 32.66. The absorption cross sections for **1**−**3** (14.66−32.66) and **7**−**9** (9.74−16.70) are enhanced compared to their ligands. However, MOFs **4**−**6** relatively do not show considerable enhancement of their two-photon absorption cross section (2.6−8.73). The two-photon excited photoluminescence spectra are obtained, and their power dependence plots are shown in Figures S30−S33. Besides their UV not indicating any absorption at 800 nm (Figure S25), the gradient of the power dependence plot is another indication that the upconversion emission observed is a two-photon absorption process. The absence of a real accessible energy level at 800 nm indicated that the absorption proceeds via a virtual state commonly observed in two-photon absorbing materials.

DOI: 10.1021/acs.chemmater.7b02417
Chem. Mater. 2017, 29, 7424−7430

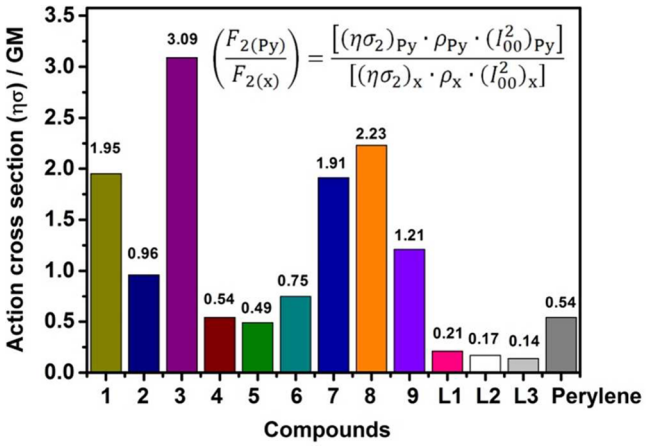

Figure 3. Estimate of the two-photon action cross section of the compounds. The formula used to compute the two-photon absorption cross section where $F_{2(Py)}$ and $F_{2(X)}$ are the measured PL strengths of perylene and compound, respectively. The integrated area below the PL spectra is used for the computation. η is the PL quantum yield, σ_2 is the two-photon absorption cross section, and $\eta\sigma_2$ is the action cross section of the compound. ρ is the sample molar concentration, and I_{00} is the peak intensity of the input laser pulse.

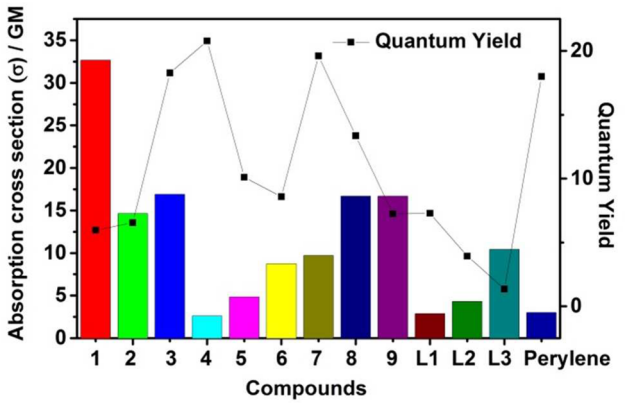

Figure 4. Two-photon absorption cross sections and quantum yields of the compounds. By knowing the quantum yield of the compounds, the absorption cross section is computed and represented by the line plot.

DISCUSSION

Upon determining their quantum yield, the two-photon absorption cross sections of the compounds are computed and compared. It is interesting to find that the trend is vastly different from their two-photon action cross sections which took into account their quantum efficiency. L3 has the highest two-photon absorption cross section among the ligands but the lowest quantum yield and two-photon action cross section among the ligands. MOF **1** has the highest two-photon absorption cross section of all the MOFs. However, due to quantum efficiency, the two-photon excited emission was the largest for MOF **3** and not MOF **1**. Although MOFs **4**−**6** are isostructural to **1**−**3**, the two-photon absorption cross sections do not follow the same trend as observed in their action cross sections. Furthermore, **7**−**9** have a different packing topology and interpentration from **1**−**3** which did not seem to affect the two-photon absorption cross section. Overall, the structural aspect did not dictate the two-photon absorption cross section of the MOF material. Rather, the ligand is critical in imbuing the MOF with a higher two-photon absorption cross section. However, it is important to point out at this stage that having large two-photon absorption cross section does not necessarily afford a large two-photon excited emission. Both the quantum yields and two-photon absorption cross sections do not exhibit comprehensible structural−property relationship. As such, the modulating effect of structure on quantum yield and two-photon absorption cross section is unclear at this point; however, the two-photon action cross sections which are an indicator of the actual brightness of the two-photon excited emission process showed discernible trends.

In general, the strength of two-photon action cross section is boosted in MOFs as compared to the individual organic spacers. The rigidifying of organic chromophores into structured MOF manifold is known to boost emission as reabsorption due to aggregation being reduced.[17,22] The emission profiles of the MOFs resemble the principle ligand used to construct them (Figure S27) indicating the two-photon process goes through the same excited state as the single photon excitation. Furthermore, the absence of the carboxylate emission is due to the strut-to-strut energy transfer[28] which occurred from the respective auxiliary carboxylate to the pyridyl ligands. It is worth noting that most MOFs have a better two-photon action cross section than the standard perylene dye. Across the ligands, the two-photon absorption fluorescence is the strongest for An2Py > AnEPy > BPEB. Although BPEB possessed a similar symmetrical acceptor−π−donor−π−acceptor (A−π−D−π−A) chemical structure, the anthracene ring came across as a better electron donor than the central benzene moiety. As such, the intramolecular charge transfer which affects the hyperpolarizability is reduced compared to An2Py and AnEPy. In addition, the dynamic rotation of the ligand[29] within the empty spaces in MOF frameworks is well-known for the anthrancene-type ligand. It is worth noting that the An2Py molecule is not perfectly planar and is torsioned at an angle of 34.88° while AnEPy is at 25.57°. The rotation of An2Py is more difficult as it has to undergo a pseudopedal-like motion.[30] In comparison, AnEPy could rotate relatively freely, which increases the likelihood of nonradiative decay. This could account for the lower absorption fluorescence observed for the ligand as well as the MOFs of AnEPy.

As compounds **1** and **2** are 4-fold interpenetrated in a similar manner, the extra double bond in the SDC ligand used to construct the MOF enables a greater degree of conjugation and hence a higher two-photon excited photoluminescence as compared to **2** stitched by BPDC. However, as the interpenetration is reduced to two as in the case of **3**, the BDC auxiliary ligand brought pairs of An2Py into alignment. The assembly of the ligand into an H-aggregate-like packing possibly accounts for the large Stoke's shifted spectra and presumably lower emission efficiency.[31] However, the locking of An2Py into a double pillared structure restricts the rotation of the ligand within the framework, enabling a reduced nonradiative decay which causes **3** to exhibit a higher two-photon excited fluorescence compared to **1** and **2**. Noting the difference in the two-photon absorption strength between An2Py and AnEPy, the property is transferred to their respective MOFs. Compounds **4**−**6** are analogues of **1**−**3** that showed lowered two-photon excited emission. The trend in which the auxiliary ligands affects the emission is also replicated.

Compounds **7** and **8** are structured with BTC as the auxiliary ligand. As discussed, both adopt the same **hms** net and the ligand's property is transferred to the MOFs. However,

DOI: 10.1021/acs.chemmater.7b02417
Chem. Mater. 2017, 29, 7424−7430

although An2Py exhibited a higher two-photon excited fluorescence than BPEB, **7**, which contains An2Py showed lower two-photon excited fluorescence compared to **8**. It is often difficult to compare across different packings as there are many interplay factors affecting the fluorescence. The tridentate ligand probably spaced An2Py ligands apart better than the bidentate ones. Despite lacking a secondary ligand for light harvesting, compound **9** showed considerable two-photon excited fluorescence as it has a void space of 40% and the ligands are well spaced in the framework reducing nonradiative decay. Interplay factors such as more space for the rotation of the ligands could reduce the fluorescence intensity, and the increased void space potentially implied the ligands are spaced further apart giving rise to reduced nonradiative decay by reabsorption during the emission process.

CONCLUSION

The structural property relationship of nine MOFs containing two-photon active ligands An2Py, AnEPy, and BPEB was reviewed in this study. An2Py and AnEPy, which have suitable A−π−D−π−A structures, exhibited higher two-photon action cross sections compared to BPEB. This nature is mostly transscribed to the MOFs they formed. Systematic variation of the auxiliary ligand lengths and the effect on the structural packing alters the two-photon absorption emission as well. Although the structural−property relationship of the compounds' two-photon action cross sections was established here, the interplay of various factors such as conjugation degree of the auxiliary ligand, ligand rotation within the frameworks, and possible void space can affect the two-photon absorption ability and the quantum efficiency to a different extent in the MOFs and may require further exploration. Designing MOFs with high two-photon absorption cross sections and quantum yields will be crucial to synthesizing efficient solid state two-photon MOF emitters. This study provides a guide for the rational design and development of new two-photon active MOF materials.

ASSOCIATED CONTENT

Supporting Information

The Supporting Information is available free of charge on the ACS Publications website at DOI: 10.1021/acs.chemmater.7b02417.

Additional characterization data, including crystal data, structure refinements, packing, PXRD patterns, TGA data, UV−vis and PL data, two-photon excited emission power dependence plot, and quantum yield emission data (PDF)

AUTHOR INFORMATION

Corresponding Author

*(J.J.V.) E-mail: chmjjv@nus.edu.sg. Fax: (+65)6779-1691.

ORCID

Venkatram Nalla: 0000-0003-4535-290X

Xiaogang Liu: 0000-0003-2517-5790

Jagadese J. Vittal: 0000-0001-8302-0733

Author Contributions

J.J.V. proposed and supervised the project. He also did the final refinements of the crystal structures. H.S.Q. and C.A.L. performed all the synthesis and characterization of ligands and MOFs. H.S.Q. performed the confocal microscopic imaging of the compounds and computed the estimated two-photon cross sections. K.Z. and X.L. helped to measure the solid-state absolute fluorescence quantum yields. V.N. performed the two-photon power dependence slope plots. The manuscript was written by H.S.Q. with input from C.A.L. and V.N. and corrected by J.J.V. and X.L.

Funding

We thank the Ministry of Education, Singapore, for financial support via NUS FRC Grant Nos. R-143-000-678-114 and R-143-000-604-112 and Singapore Ministry of Education Academic Research Fund Tier 3 (Grant MOE2011-T3-1-005).

Notes

The authors declare no competing financial interest.

CCDC 1551659 to 1551664 (**2**−**4** and **7**−**9**) contain the supplementary crystallographic data for this paper. These data can be obtained free of charge from the Cambridge Crystallographic Data Centre via www.ccdc.cam.ac.uk/data_request/cif.

ACKNOWLEDGMENTS

We express gratitude towards Ms. Geok Kheng Tan and Bruno Donnadieu for X-ray data collection and initial refinements of the crystal structures. We express our thanks to the CBIS Confocal Microscopy Centre of the Life Sciences NUS for their support of the confocal microscopy measurements. Lastly, we appreciate the help of NUS CMMAC lab technologists for all their help in this project. H.S.Q thanks NUS NGS for providing the scholarship.

REFERENCES

(1) Burstein, E. Anomalous optical absorption limit in InSb. *Phys. Rev.* **1954**, *93*, 632−633.

(2) Huang, M. H.; Mao, S.; Feick, H.; Yan, H.; Wu, Y.; Kind, H.; Weber, E.; Russo, R.; Yang, P. Room-temperature ultraviolet nanowire nanolasers. *Science* **2001**, *292*, 1897−1899.

(3) Iliopoulos, K.; Krupka, O.; Gindre, D.; Salle, M. Reversible Two-photon optical data storage in coumarin-based copolymers. *J. Am. Chem. Soc.* **2010**, *132*, 14343−14345.

(4) Xu, C.; Zipfel, W.; Shear, J. B.; Williams, R. M.; Webb, W. W. Multi-photon fluorescence excitation: New spectral windows for biological nonlinear microscopy. *Proc. Natl. Acad. Sci. U. S. A.* **1996**, *93*, 10763−10768.

(5) Helmchen, F.; Denk, W. Deep tissue two-photon microscopy. *Nat. Methods* **2005**, *2*, 932−940.

(6) Albota, M.; Beljonne, D.; Brédas, J. L.; Ehrlich, J. E.; Fu, J. Y.; Heikal, A. A.; Hess, S. E.; Kogej, T.; Levin, M. D.; Marder, S. R.; McCord-Maughon, D.; Perry, J. W.; Röckel, H.; Rumi, M.; Subramaniam, G.; Webb, W. W.; Wu, X. L.; Xu, C. Design of organic molecules with large two-photon absorption cross sections. *Science* **1998**, *281*, 1653−1656.

(7) Levine, B. F. Donor-acceptor charge transfer contributions to the second order hyperpolarizability. *Chem. Phys. Lett.* **1976**, *37*, 516−520.

(8) Sheng, N.; Liu, D.; Wu, J.; Gu, B.; Wang, Z. Y.; Cui, Y. P. Donor-π-acceptor type porphyrins with large two-photon absorption cross section. *Dyes Pigm.* **2015**, *119*, 116−121.

(9) Ye, C. Q.; Zhou, L. W.; Wang, X. M.; Liang, Z. Q. Photon upconversion: from two photon absorption (TPA) to triplet-triplet annihilation (TTA). *Phys. Chem. Chem. Phys.* **2016**, *18*, 10818−10835.

(10) Nakano, M.; Kishi, R.; Ohta, S.; Takahashi, H.; Kubo, T.; Kamada, K.; Ohta, K.; Botek, E.; Champagne, B. Relationship between third-order nonlinear optical properties and magnetic interactions in open-shell systems: A new paradigm for nonlinear optics. *Phys. Rev. Lett.* **2007**, *99*, 033001.

(11) Ohta, S.; Nakano, M.; Kubo, T.; Kamada, K.; Ohta, K.; Kishi, R.; Nakagawa, N.; Champagne, B.; Botek, E.; Takebe, A.; Umezaki, S.;

DOI: 10.1021/acs.chemmater.7b02417
Chem. Mater. 2017, 29, 7424−7430

Nate, M.; Takahashi, H.; Furukawa, S.; Morita, Y.; Nakasuji, K.; Yamaguchi, K. Theoretical study on the second hyperpolarizabilities of phenalenyl radical systems involving acetylene and vinylene linkers: Diradical character and spin multiplicity dependences. *J. Phys. Chem. A* **2007**, *111*, 3633−3641.
(12) Nakano, M.; Kishi, R.; Nitta, T.; Kubo, T.; Nakasuji, K.; Kamada, K.; Ohta, K.; Champagne, B.; Botek, E.; Yamaguchi, K. Second Hyperpolarizability (γ) of Singlet Diradical System: Dependence of γ on the Diradical Character. *J. Phys. Chem. A* **2005**, *109*, 885−891.
(13) Fukuda, K.; Nakano, M. Intramolecular Charge Transfer Effects on the Diradical Character and Second Hyperpolarizabilities of Open-Shell Singlet X−π−X (X = Donor/Acceptor) Systems. *J. Phys. Chem. A* **2014**, *118*, 3463−3471.
(14) Kitagawa, S.; Kitaura, R.; Noro, S. Functional porous coordination polymers. *Angew. Chem., Int. Ed.* **2004**, *43*, 2334−2375.
(15) Chen, B. L.; Ockwig, N. W.; Millward, A. R.; Contreras, D. S.; Yaghi, O. M. High H_2 adsorption in a microporous metal-organic framework with open metal sites. *Angew. Chem., Int. Ed.* **2005**, *44*, 4745−4749.
(16) Li, J. R.; Sculley, J.; Zhou, H. C. Metal-organic frameworks for separations. *Chem. Rev.* **2012**, *112*, 869−932.
(17) Cui, Y. J.; Yue, Y. F.; Qian, G. D.; Chen, B. L. Luminescent functional metal-organic frameworks. *Chem. Rev.* **2012**, *112*, 1126−1162.
(18) Seo, J. S.; Whang, D.; Lee, H.; Jun, S. I.; Oh, J.; Jeon, Y. J.; Kim, K. A homochiral metal-organic porous material for enantioselective separation and catalysis. *Nature* **2000**, *404*, 982−986.
(19) Batten, S. R.; Murray, K. S. Structure and magnetism of coordination polymers containing dicyanamide and tricyanomethanide. *Coord. Chem. Rev.* **2003**, *246*, 103−130.
(20) Heintz, R. A.; Zhao, H.; Ouyang, X.; Grandinetti, G.; Cowen, J.; Dunbar, K. R. New insight into the nature of Cu(TCNQ): Solution routes to two distinct polymorphs and their relationship to crystalline films that display bistable switching behavior. *Inorg. Chem.* **1999**, *38*, 144−156.
(21) Yu, J.; Cui, Y.; Wu, C.; Yang, Y.; Chen, B.; Qian, G. Two-Photon Responsive Metal−Organic Framework. *J. Am. Chem. Soc.* **2015**, *137*, 4026−4029.
(22) Quah, H. S.; Chen, W.; Schreyer, M.; Yang, H.; Wong, M. W.; Ji, W.; Vittal, J. J. Multiphoton harvesting metal-organic frameworks. *Nat. Commun.* **2015**, *6*, 7954. Quah, H. S.; Chen, W.; Schreyer, M.; Yang, H.; Wong, M. W.; Ji, W.; Vittal, J. J. Multiphoton harvesting metal-organic frameworks. *Nat. Commun.* **2015**, *6*, 7954.
(23) Zhao, H.; Xia, Q.; Xing, H.; Chen, D.; Wang, H. Construction of pillared-layer MOF as efficient visible-light photocatalysts for aqueous Cr(VI) reduction and dye degradation. *ACS Sustainable Chem. Eng.* **2017**, *5*, 4449−4456.
(24) Liu, Y.; Chen, D.; Li, X.; Yu, Z.; Xia, Q.; Liang, D.; Xing, H. Visible-light-induced controlled radical polymerization of methacrylates mediated by a pillared-layer metal-organic framework. *Green Chem.* **2016**, *18*, 1475−1481.
(25) Nugent, P.; Belmabkhout, Y.; Burd, S. D.; Cairns, A. J.; Luebke, R.; Forrest, K.; Pham, T.; Ma, S.; Space, B.; Wojtas, L.; Eddaoudi, M.; Zaworotko, M. J. Porous materials with optimal adsorption thermodynamics and kinetics for CO2 separation. *Nature* **2013**, *495*, 80−84.
(26) Makarov, N. S.; Drobizhev, M.; Rebane, A. Two-photon absorption standards in the 550−1600 nm excitation wavelength range. *Opt. Express* **2008**, *16*, 4029−4047.
(27) Katoh, R.; Suzuki, K.; Furube, A.; Kotani, M.; Tokumaru, K. Fluorescence Quantum Yield of Aromatic Hydrocarbon Crystals. *J. Phys. Chem. C* **2009**, *113*, 2961−2965.
(28) Lee, C. Y.; Farha, O. K.; Hong, B. J.; Sarjeant, A. A.; Nguyen, S. T.; Hupp, J. T. Light-harvesting metal-organic frameworks (MOFs): efficient strut-to-strut energy transfer in bodipy and porphyrin-based MOFs. *J. Am. Chem. Soc.* **2011**, *133*, 15858−15861.
(29) Schneemann, A.; Bon, V.; Schwedler, I.; Kaskel, S.; Fischer, R. A.; Senkovska, I. Flexible metal-organic frameworks. *Chem. Soc. Rev.* **2014**, *43*, 6062−6069.
(30) Peedikakkal, A. M. P.; Vittal, J. J. Solid-state photochemical [2 + 2] cycloaddition in a hydrogen-bonded metal complex containing several parallel and crisscross C═C bonds. *Chem. - Eur. J.* **2008**, *14*, 5329−5334.
(31) Zhai, D.; Xu, W.; Zhang, L.; Chang, Y. T. The role of "disaggregation" in optical probe development. *Chem. Soc. Rev.* **2014**, *43*, 2402−2411.

DOI: 10.1021/acs.chemmater.7b02417
Chem. Mater. 2017, 29, 7424−7430